

Article

Development of Non-Contact Measurement Techniques for Concrete Elements Using Light Detection and Ranging

Thanh Thi Pham, Doyun Kim, Ukyong Woo, Su-Gwang Jeong  and Hajin Choi * 

Structural Engineering/Building Materials, Soongsil University, 369 Sangdo-ro, Seoul 06978, Republic of Korea; phamthithanh02101997@gmail.com (T.T.P.); hie1253@soongsil.ac.kr (D.K.); dnrdyd0379@gmail.com (U.W.); sgjeong@ssu.ac.kr (S.-G.J.)

* Correspondence: hjchoi@ssu.ac.kr

Abstract: The objective of this study is to develop a monitoring algorithm that measures the displacement of concrete structures using light detection and ranging (LiDAR). The suggested method is based on non-contact measurements providing 3D point clouds of the scanning area with high resolution. This overcomes the limitation of traditional contact-type and point-based measurement methods such as linear variable differential transformer (LVDT) and strain gauge. The developed algorithm enables one to track the boundaries of a concrete specimen and measures the vertical or lateral displacement. To demonstrate that displacement in the horizontal and vertical direction can be measured irrespective of the field of view (FOV), two different concrete specimens were constructed where gradually increasing vertical or lateral loads were applied. Then, the displacements were monitored using the set of LVDT and LiDAR for the correlation analysis. The results demonstrated a high accuracy of 98~99% correlation in comparison between LVDT and LiDAR.

Keywords: 3D point clouds; light detection and ranging (LiDAR); structural health monitoring (SHM); concrete



Citation: Pham, T.T.; Kim, D.; Woo, U.; Jeong, S.-G.; Choi, H. Development of Non-Contact Measurement Techniques for Concrete Elements Using Light Detection and Ranging. *Appl. Sci.* **2023**, *13*, 13025. <https://doi.org/10.3390/app132413025>

Academic Editor: Wael Zatar

Received: 9 November 2023

Revised: 29 November 2023

Accepted: 4 December 2023

Published: 6 December 2023



Copyright: © 2023 by the authors. Licensee MDPI, Basel, Switzerland. This article is an open access article distributed under the terms and conditions of the Creative Commons Attribution (CC BY) license (<https://creativecommons.org/licenses/by/4.0/>).

1. Introduction

Concrete is a widely used material in construction and civil engineering. Reinforced concrete (RC) is a composite system, consisting of concrete that is strong in compressive force and a steel bar that is strong in tensile force. The RC structure has been applied to various buildings and bridges due to its high strength, durability, and fire resistance. However, sudden collapses of reinforced concrete structures at construction sites, often resulting in numerous casualties and significant property damage, are typically due to insufficient curing periods or loads exceeding the concrete's capacity. Therefore, testing methods for measuring strength and internal cracks to prevent accidents caused by concrete include the rebound method, ultrasonic velocity method, and infrared ray measurement method. Although periodic monitoring equipment is used for detecting cracks and deterioration in existing concrete structures, there is an increasing need for real-time monitoring of displacement and deformation in the field of structural health monitoring [1].

Structural health monitoring (SHM) is significant in civil infrastructure for evaluating structural behavior in the field [2–8]. Sensors used for monitoring the deformation of concrete structures are conventionally attached types (e.g., linear variable differential transformer (LVDT) and strain gauge). These sensors have the following disadvantages. Strain gauges have the disadvantage of requiring the surface of the rebar to be prepared in advance, necessitating its attachment to the rebar before the concrete is poured. LVDT has the disadvantage that an additional structure is required to fix the sensor in a way that contacts the surface of the concrete structure. In addition, since all of these sensors operate only on one axis, a large number of sensors are required to know the overall deformation of the structure, which requires a lot of time and manpower to install in advance. In order to overcome these disadvantages, it is necessary to introduce a new measurement method.

A light detection and ranging (LiDAR) instrument emits a laser pulse to a target, measures the return time, and converts these data into point clouds represented as three-dimensional coordinate values. LiDAR is a contactless scan method, but it is often used in various fields due to its high resolution and short scan time. LiDAR is primarily used for perception and mapping. It helps a vehicle understand its surroundings by creating a detailed 3D representation of the environment, detecting objects (such as other vehicles, pedestrians, and obstacles), and providing depth information for localization and navigation. In the case of crack detection in concrete surfaces, LiDAR is employed as a non-destructive testing (NDT) method to identify cracks, fissures, or other irregularities in concrete. Its purpose is to assess the structural integrity of the concrete and identify areas that may require repair or maintenance. Jo et al. (2018) introduced a method to calculate deformation and strain in steel plates using 3D coordinate data obtained from LiDAR. The estimated strains were compared to the measured values from strain gauges. The comparison results indicated that the strain trends for all cases were similar [9]. Cabaleiro et al. (2015) developed a new algorithm for 3D modeling and deformation to verify the geometry of the beams or determine whether a beam is acceptable or not in terms of deformation. A realistic 3D modeling of the deformed beam was performed automatically and reliably. However, this approach is only valid for situations in which the modeled structures are assumed to behave elastically [10]. Sun et al. (2016) presented non-contact optical sensing using 3D stereo vision to measure the deformation of asphalt mixture concrete. The results were validated with LVDT data. The absolute average differences among the measured data using LVDT, finite element analysis, and the proposed stereovision method exhibited no significant difference [11]. Maru et al. (2020) investigated methods for estimating the deflection of structures based on LiDAR data. The proposed approach was validated with an indoor experiment by inducing artificial deflection on a simply supported beam. The deflection value at various points was validated using LVDT. The results indicated that the error between two methods is negligible [12]. Kang et al. (2019) showed a novel RGB-D SLAM using LiDAR point cloud data as the guidance for indoor 3D scene construction and navigation. The proposed method was tested for long-distance tracking in two different large indoor scenarios. The experimental results indicated that the standard deviation of the 3D map construction is 10 cm in a mapping distance of 100 m, compared with the LiDAR ground truth. Further, the relative cumulative error of the camera in closed-loop experiments is 0.09%, which is two times less than that of the typical SLAM algorithm (3.4%) [13]. Kim et al. (2022) presented a 2D LiDAR sensor-based system for measuring retaining wall deformation. Laboratory experiments were performed using a simulated deformation model to evaluate the displacement measurement performance of the system, which had a root-mean-square error of 2.82 mm at approximately 20 m. The economic feasibility of the system was analyzed, which revealed that the system was economically feasible, with a benefit/cost ratio and breakeven point of 3.52 and 2.71 years [14]. Lee et al. (2023) mentioned an experiment using LiDAR to survey for soft ground settlement measurements at a large land reclamation site, showing a very large settlement up to 10 m with 6.23% root-mean-square error in terms of vertical accuracy, predicted long-term settlement, and consolidation [15]. Thus, LiDAR is totally reliable for measuring the displacement of building structures.

However, two major disadvantages of using LiDAR equipment for construction site monitoring are its high cost and the large volume of 3D data it generates. Commercial high-price LiDAR is usually used for applications requiring high accuracy, such as autonomous vehicles, surveying, mapping, aerospace, industrial automation, and environmental monitoring. Moreover, commercial LiDAR can measure large areas with high resolution and has better noise filtering capabilities. However, commercial high-price LiDAR measures more unnecessary data than region of interest because most LiDAR equipment supports 360° scanning. On the other hand, low-cost LiDAR are to be used to meet economic feasibility and observation targets, such as concrete surfaces and concrete wall. Practically, the degree of noise on the surface and edges will increase the error range for measured data and

reduce reliability. Nevertheless, noise of the measured data can be revised by applying a line or plane fitting to the measured point cloud data, which improves noise level on the edges or planes within the point clouds. The use of low-cost LiDAR significantly enhances cost-effectiveness for projects. Generally, the cost for commercial high-price LiDAR is about USD 5000 while low-cost LiDAR is only USD 500, which basically saves up to 90%.

In this study, it was presented that a real-time monitoring system for concrete structures was constructed using LiDAR equipment and a displacement extraction algorithm. The reliability of the extracted data was verified through simultaneous measurement and cross-analysis of a traditional LVDT and a LiDAR. In addition, linear fitting was applied to correct the instrumentation noise generated by non-contact sensors, thereby improving the accuracy of the extracted displacement. As such, the algorithm to which linear fitting was applied derived accurate quantitative values for the displacement of the structure through data processing analysis.

2. Methodology

2.1. Measurement Mechanism of LiDAR

LiDAR is a technology that uses eye-safe laser beams to produce a 3D map of the surveyed environment. LiDAR is applied in a wide variety of industries, such as the automotive industry, infrastructure, robotics, the trucking industry, the industrial industry, mapping, and many more [16,17]. LiDAR releases pulsed light waves into the surrounding area, and these pulses return to the sensor after bouncing off nearby objects. The sensor determines the distance traveled by each pulse by measuring the time it takes for it to return to the sensor. A real-time 3D map of the environment is produced by repeating this procedure millions of times per second. In this study, an Intel[®] Realsense[™] LiDAR Camera L515 was used as the LiDAR device (Figure 1). The device has the advantage of being able to simultaneously measure both point cloud and RGB data because it includes both an image camera and an IR camera. The IR camera section comprises an IR transmitter, which fires an infrared laser with a wavelength of 860 nm at the target, and an IR receiver, which detects the reflected laser. The built-in depth camera can collect 1024×768 point cloud data points and measure distances from 0.25 m up to a maximum of 9 m. The image camera can capture 1280×720 high-definition RGB data points, and its detailed specifications are shown in Table 1.

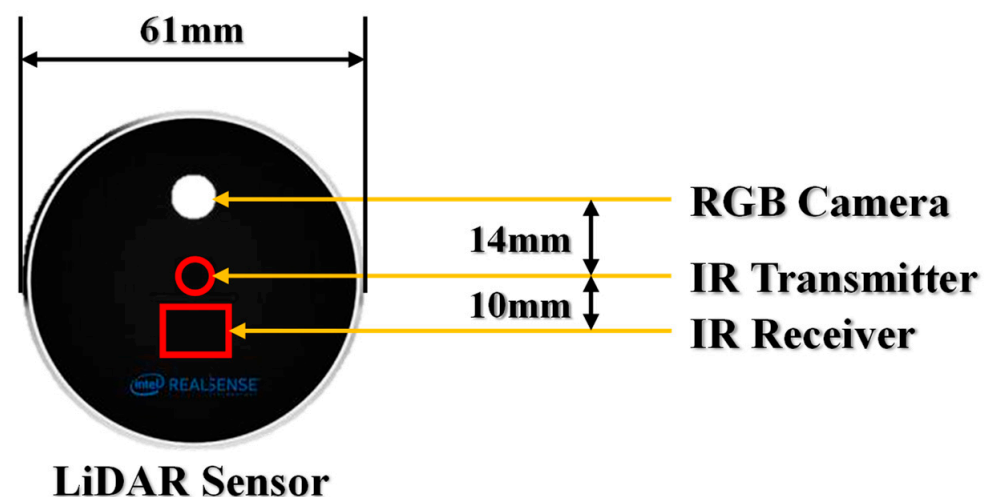


Figure 1. LiDAR equipment used in the experiment.

Table 1. LiDAR equipment specifications.

Instrument Type	Value
Available range of depth distance	250~9000 mm (only interior)
Depth accuracy	5 mm
Depth field of view (FOV)	70° (H) × 55° (V)
Depth output resolution	1024 (H) × 768 (V)
RGB frame resolution	1280 (H) × 720 (V)
Maximum measurable speed	30 Hz

2.2. Development of Displacement Extraction Algorithm from Point Clouds

The first step in non-contact displacement extraction in a concrete experiment is to select labels corresponding to concrete using the Density-based spatial clustering of applications with noise (DBSCAN) algorithm and remove other clusters. DBSCAN is one of the most widely used methods for labeling point clouds and is a non-parametric algorithm that identifies adjacent points within a specified threshold distance as one label. Since DBSCAN forms a non-linear cluster, it can build a cluster for any non-linearity, and it is effective in removing noise by recognizing outliers outside the threshold distance as another cluster [18,19]. By applying the DBSCAN algorithm, each classified cluster is given a labeling number consisting of a number that gradually increases from one, and then a Region of Interest (ROI) extraction mask is produced by extracting a labeling number corresponding to a concrete coordinate point. The ROI extraction mask designates the concrete area as 1 and other labeled parts (side-attached LVDT sensors, people, background, noise) as 0, and is applied to the raw data of the point cloud to remove unnecessary parts. A flowchart of the applied algorithm is illustrated in Figure 2.

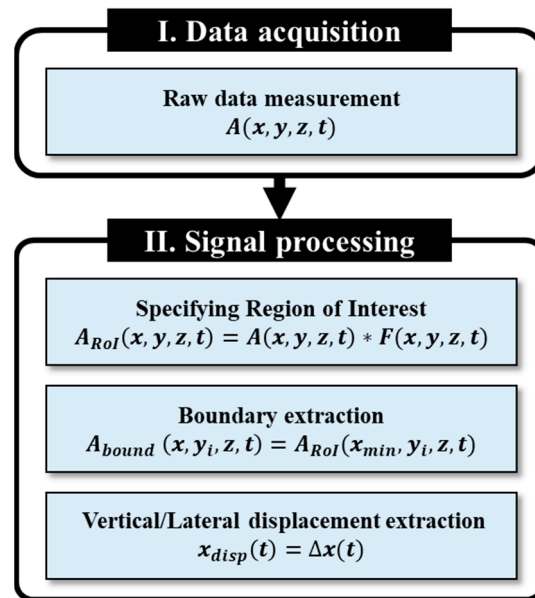


Figure 2. An algorithm of displacement extraction from point clouds.

Despite the expectation that the edge of concrete would be linear, the point clouds extracted from LiDAR exhibit a nonlinear trend due to noise, as shown in Figure 3. To correct the noise in the measurement data, regression analysis was employed [20]. Since RC structures typically have a simply linear structural behavior with respect to rigid body motion, one-dimensional linear fitting was applied to correct the data of the distorted point cloud and derive new left boundary points. The processing of the extraction was repeated for all data measured over the structural loading test.

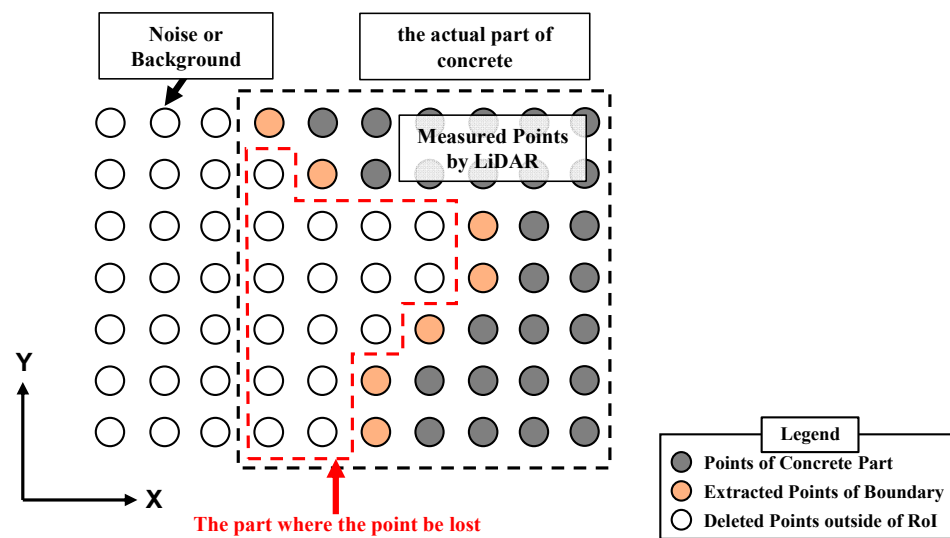


Figure 3. An algorithm designed to extract edges from a point cloud and a diagram illustrating the measurement data discrepancies with the actual concrete surface.

The collected point cloud data may contain inaccurate points, known as mixed-pixels, due to discontinuities in space at the interface of an object. Tang et al. (2007) and Tang et al. (2009) reported that LiDAR emits a laser with a certain width of diameter to determine distance from the target [21,22]. The diameter of the laser beam is designed to be small, often in the range of a few millimeters to a centimeter. If the laser point reflects off both foreground and background surfaces simultaneously within the diameter of one laser point, the distance measurement will be incorrect. Additionally, micro-angle changes at the edge of the concrete can cause point distortion or omission. Point distortion or noise is problematic for displacement extraction from concrete surfaces; however, increasing the resolution of the point cloud can be a solution. In this study, the resolution of the point cloud in the vertical and horizontal axes was less than 1 mm, as shown in Table 2, which is less than the resolution of LVDT. Therefore, the error rate of the displacement measurement in concrete structures is possibly minimized in this study.

Table 2. Resolution of LiDAR measurement in this study.

Types	Values
Horizontal resolution	~0.96 mm
Vertical resolution	~0.97 mm
Distance between specimen and LiDAR	800 mm

3. Testing Set-Up and Data Acquisition

3.1. Experiments to Measure Horizontal Displacement

3.1.1. Precast Concrete Walls Information

Reinforced concrete walls were erected to assess the feasibility of real-time lateral displacement monitoring with LiDAR equipment. The study employed two types of precast (PC) walls in its construction, as illustrated in Figure 4. Figure 4a showcases Wall A, consisting of four PC walls each measuring 1550 mm (B) × 800 mm (H) × 200 mm (T), together resulting in a total height of 3200 mm. Shear reinforcement bars were exclusively installed on the PC wall located on the first level, which encountered the greatest degree of loading. The manufactured PC wall was fastened to a foundation of 2400 mm (B) × 550 mm (H) × 800 mm (T) at the bottom and a force beam of 1550 mm (B) × 400 mm (H) × 350 mm (T) at the top. Figure 4b showcases Wall B, which features a 450 mm (B) × 600 mm (H) opening between a 350 mm (B) × 800 mm (H) wall and a 750 mm (B) × 800 mm (H) wall. This opening enables a 200 mm high beam to connect the asymmetric left and right walls. Wall B was constructed

by stacking four separate PC walls, with the foundation and force beam matching the size of Wall A. An actuator was situated in contact with the right center of the force beam of each experimental unit and we applied a lateral load at a height of 3375 mm from the foundation. A primary LVDT labeled as number 1 was installed at the same height as the actuator of each experimental unit to measure the displacement of the wall structure due to lateral load forces.

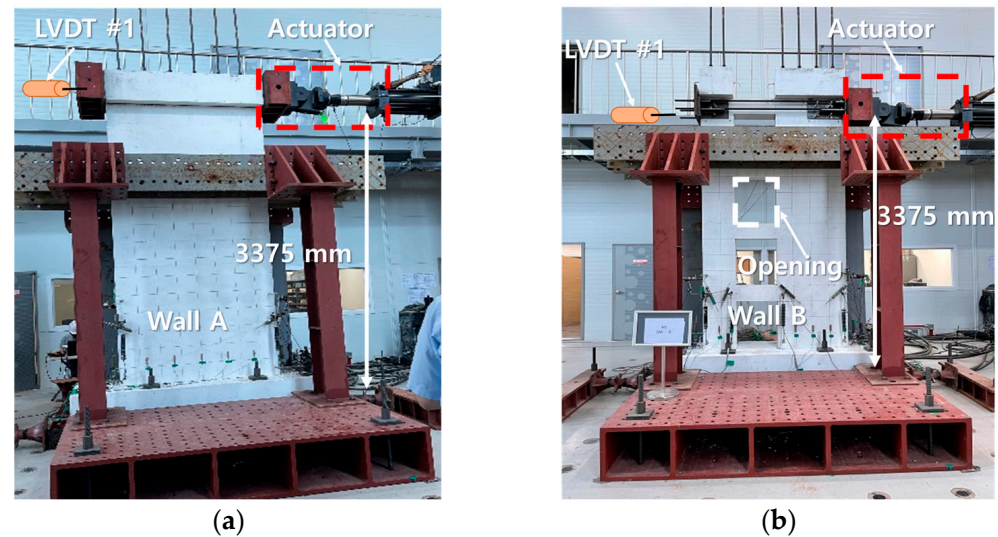


Figure 4. Precast concrete walls designed to withstand lateral loads include the following: (a) a conventional uniform flat wall and (b) a wall featuring 450 × 600 openings.

The lateral displacement applied was planned as depicted in Figure 5. The force displacement's absolute value ranged from 0.9 mm to 200 mm for approximately three hours. Three cycles were performed in both the compression and tension directions for the same displacement, and a displacement 135% larger than the previous displacement was repeated until the maximum displacement was reached.

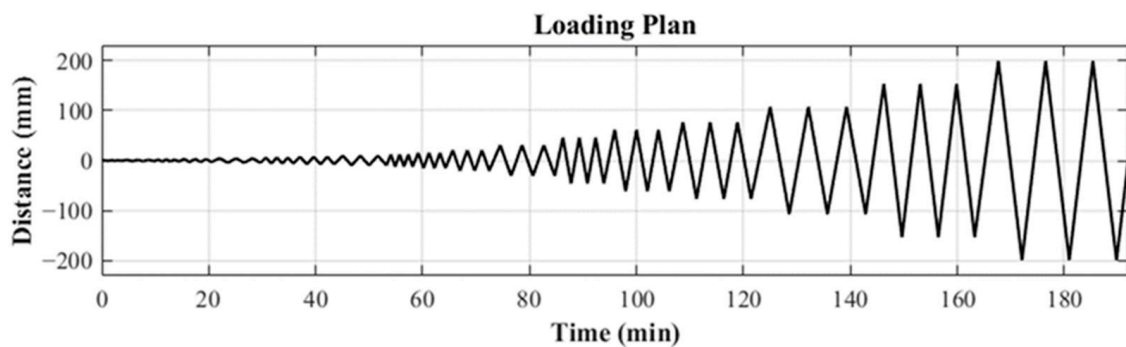


Figure 5. Loading plan for concrete wall.

3.1.2. Lateral Displacement Measurement Using LiDAR

LVDT sensors were mounted on one side of the concrete wall, while the opposite surface was scanned using LiDAR as shown in Figure 6. To use the LiDAR equipment, installation of the Intel Realsense SDK 2.0 software is necessary. This exclusive software, shared by Intel, is GUI-based and does not allow for detailed variable adjustment. For instance, the scanning frequency is fixed at 30 Hz, resulting in a high capacity charge due to the measurement data that is more than necessary. To address this, MATLAB-based measurement software with adjustable scanning intervals was created using a source code provided by Intel. This allowed for the collection of point cloud data with three-dimensional coordinates of (x, y, z) and RGB data. The scanning interval within the software was also

adjustable, and the concrete object was measured using LiDAR with a 15 s interval setting. The set-up for surface laser scanning of concrete using LiDAR, such as that shown in Figure 6, is simple, and it can save time and manpower. In addition, if only the measurable range is observed, the distance between the LiDAR equipment and the wall does not need to be precisely adjusted. Of course, if the distance becomes too far, it is not recommended because the resolution for the point spacing decreases. Figure 7 shows the RGB data and point cloud data obtained by measuring Wall A and Wall B using LiDAR before applying the load.



Figure 6. An example of non-contact measurement of displacement using LiDAR.

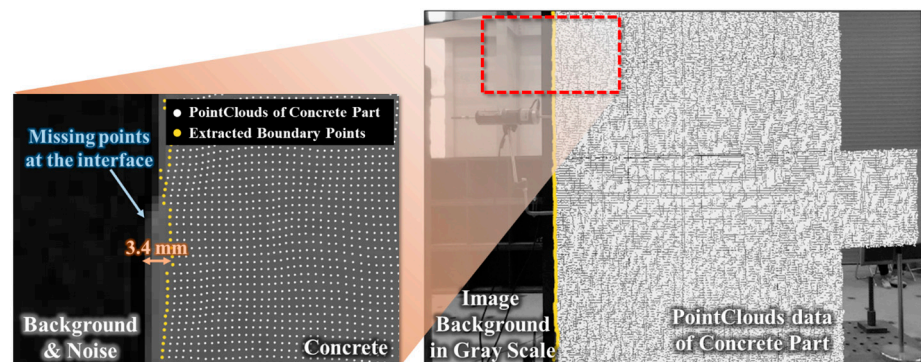


Figure 7. Combined image of measured grayscale RGB and point cloud data; some points are lost due to noise at the edges of the LiDAR equipment.

Line fitting was used to reduce noise in the point cloud data. The left boundary of the concrete wall was found to be linear, and the point cloud was reconstructed using the 1D line fitting method. In Figure 7, the orange points represent the left boundary point clouds of the concrete extracted from the raw data, the orange line is a straight line fitted based on the extracted point cloud, and the blank area on the right should be where the original concrete surface is located. The outlier points, which deviated up to 11 mm, were removed through 1D line fitting. The lateral displacement monitoring test for concrete walls resulted in the extraction of displacement data from LVDT #1 and LiDAR measurements calculated using the developed algorithm. The data were analyzed by converting them to a drift ratio for quantitative analysis. Figures 8 and 9 show the drift ratio results for Wall A and Wall B, respectively.

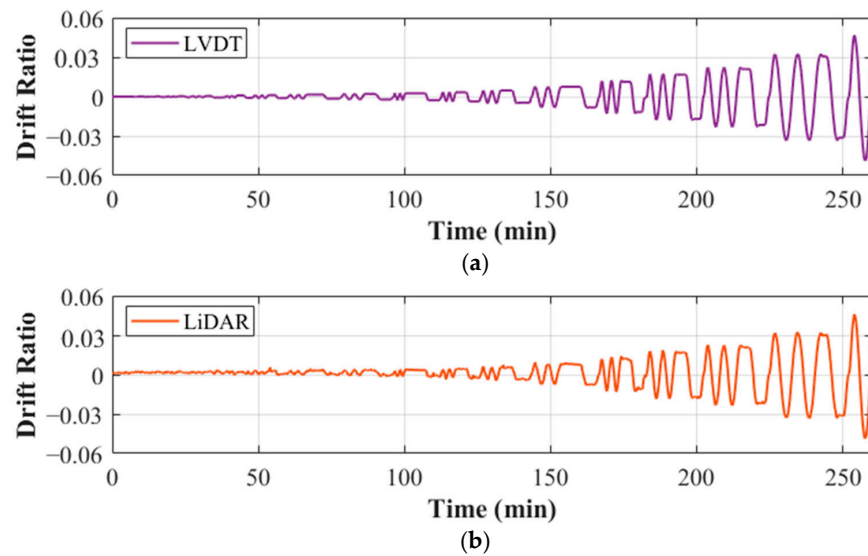


Figure 8. Drift ratio from Wall A: (a) using LVDT and (b) using LiDAR.

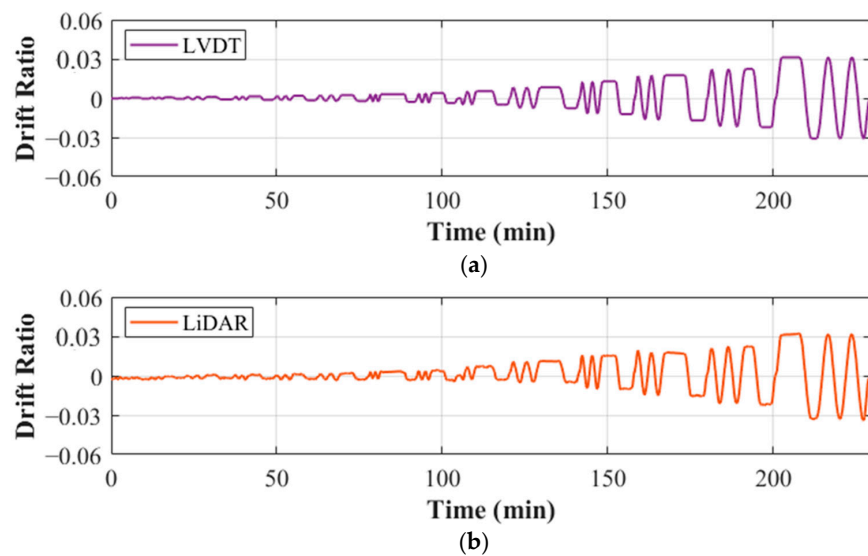


Figure 9. Drift ratio from Wall B: (a) using LVDT and (b) using LiDAR.

3.2. Experiments to Measure Vertical Displacement

3.2.1. Specimen Information

The proposed method was also employed to measure the vertical displacement of PC test specimens [23]. The test specimens were constructed to simulate the progressive collapse of the PC structures frequently used in Korea. In this study, precast concrete simple supported connection (PC-P) and precast concrete continuous supported connection (PC-C) were selected with the same design parameter: a center-to-center span of 3000 mm, a net span of 2600 mm, a story height of 2000 mm, beam dimensions of 300 mm in width and 300 mm in depth, column dimensions of 400 mm in width and 300 mm in depth, and a bracket length of 200 mm.

Figure 10a illustrates the details of PC-C with a continuous joint. PC-C is a continuously supported connection specimen that is connected between precast concrete elements, and there is no intended relative movement or rotation between the elements. The green line is a continuous bar, and the purple line is a hook bar used to connect the beam and column. These connections are used to transfer both vertical and horizontal loads between the connected elements and are typically found in structural systems where rigidity and load transfer efficiency are important. In PC beams, the bottom rebar ratio was $\rho = 0.51\%$ (2-D16

rebars). As a connection detail, the bottom rebars in PC beams were extended outward to provide anchorage, with the required bar development length (i.e., $l_d = 350$ mm). A single $\phi 15.2$ strand (i.e., diameter of $d_b = 15.2$ mm and cross-sectional area of $A_s = 138.7$ mm²) was positioned at a depth of 240 mm to apply the prestressing force. A prestressing jacking force of $F_{pe} = 205$ kN (80% of the tensile strength of the tendon, $f_{pu} = 1860$ MPa) was applied via pretension before pouring the concrete. The prestressing tendon was cut when the compressive strength of the concrete reached 30 MPa. The PC beam was placed on the PC column bracket and fixed by bolting with two D19 dowel bars (with a diameter of $d_b = 19.1$ mm and cross-sectional area of $A_s = 286.5$ mm²) extended from the bracket. The dowel bars were anchored into the PC column with a development length of 300 mm. Non-shrink mortar was used to fill the anchor holes of the dowel bars and the gaps between the PC beams and PC columns. Once the PC beams were positioned on the PC column bracket, the continuous top rebars of the topping were installed. The top bar ratio was $\rho' = 1.02\%$. The topping concrete was cast into the area encompassing the net span and the beam–column joint. At the mid-span of the beam, the nominal flexural strength for the positive moment (M_n^+) was calculated as 130 kN-m. At the both ends of the beam, the nominal flexural strength was calculated as 78 kN-m for the positive moment (M_n^-), and 135 kN-m for the negative moment, ignoring the effect of the prestressing force.

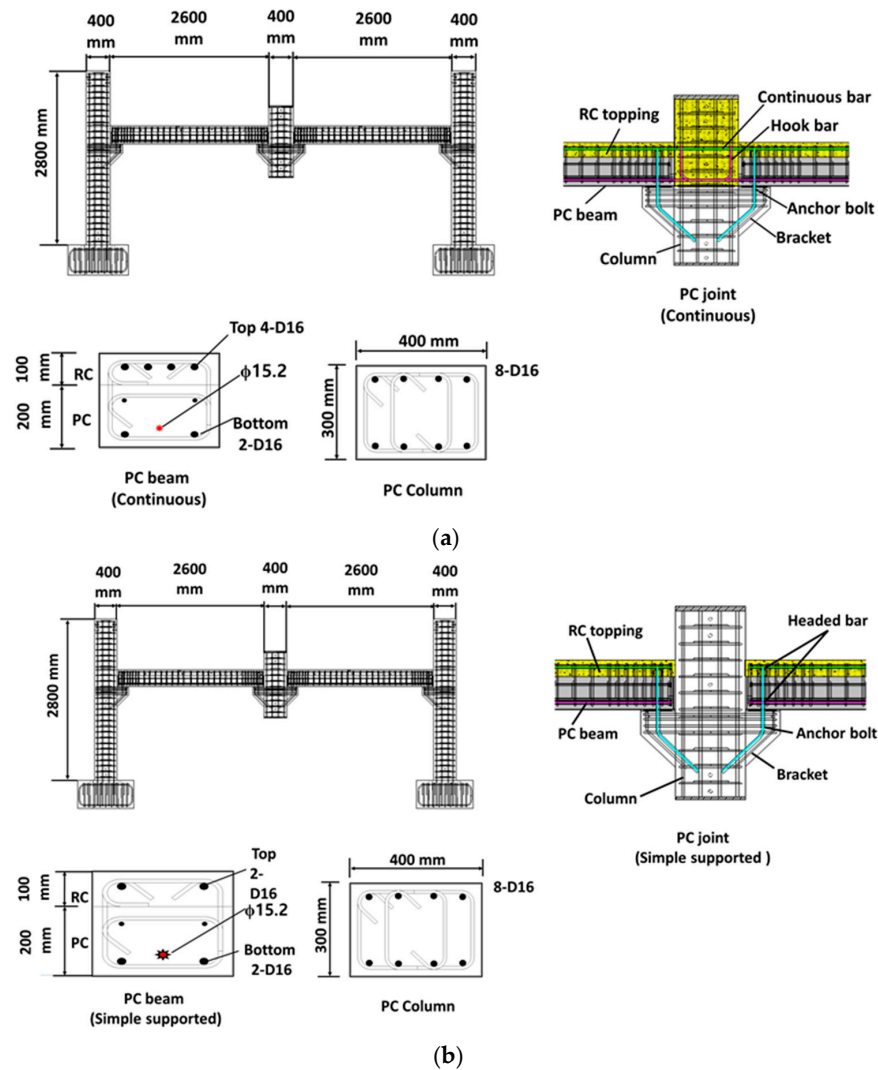


Figure 10. The details of PC specimens. (a) PC-C specimen; (b) PC-P specimen.

Figure 10b illustrates the specific characteristics of PC–P with a pinned joint. PC–P is a simply supported connection specimen that is connected between two precast concrete elements where one element is supported by the other in a manner that allows for relative movement between them. The rebar details in PC beam and PC column were the same as those in PC–C, except that the bottom and top rebars (represented by the green and purple lines) were not continuous at the beam–column joint. The top and bottom bars of the PC beam were anchored at the ends of the PC beam using headed bars. Further, topping concrete was only poured in the net span region. In the topping concrete, the top bar ratio was 0.51%. The nominal flexural strength of the beam at the mid-span was $M_n^+ = 130 \text{ kN}\cdot\text{m}$ for the positive moment. However, the nominal flexural strength for the negative moment could not be achieved at both ends of the beam since the top and bottom bars of the beams were not continuous in the beam–column joint.

3.2.2. Vertical Displacement Measurement Using LiDAR

To verify the proposed measurement method, the displacement of the PC test specimens was measured during the vertical static loading tests. Figure 11 shows the test set-up of the specimen. In the test, the LiDAR devices were conveniently installed 800 mm in front of the test specimen, a distance unaffected by potential damage and failure of the specimen. On the other hand, twenty LVDTs were directly installed on the specific location of the specimen surface, and they required many complicated assistant devices. Thus, when severe damage occurred, the errors in measurement were significantly affected. In this study, the center of the specimen, including the joint with two beams, was selected to measure the vertical displacement. An Intel LiDAR L515 was used to collect data in the form of Bin files and JPEG images. In the PC–C specimen, a total of 1923 bin files and 1923 JPEG images were collected with image qualities of 1280×720 pixels. In the PC–P specimen, a total of 883 bin files and 883 JPEG images were collected with image qualities of 1280×720 pixels. The average LVDT1 (L1) and LVDT2 (L2) was used for validation with LiDAR. On the other hand, the displacement of the test specimens was measured simultaneously with LiDAR processing time.

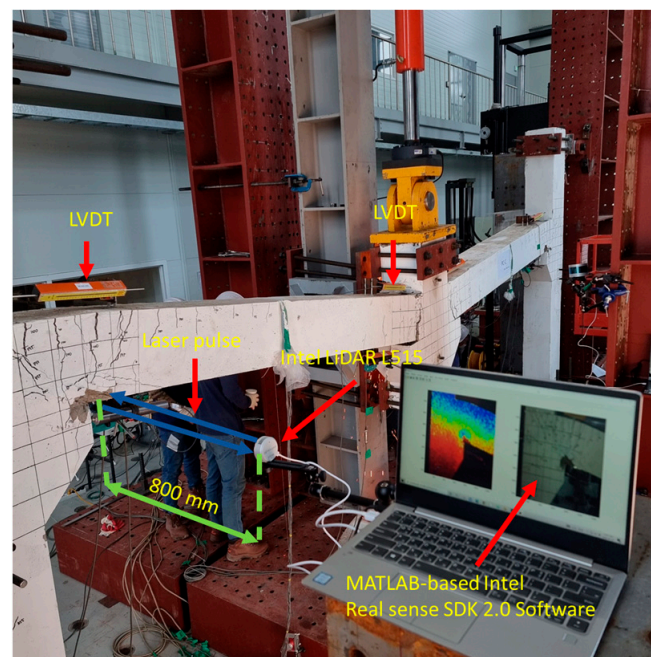


Figure 11. Conventional displacement (LVDT) set-up.

Using the proposed LiDAR method, the vertical displacement of the beam–column joint and the beam end rotation angle were measured. Firstly, the boundary of the specimen was extracted from the original point cloud data by applying data filters. The M-estimator Sample Consensus (MSAC) algorithm is a robust parameter estimation method commonly used in computer vision and image processing tasks. It is an extension of the Random Sample Consensus (RANSAC) algorithm, designed to handle data with outliers and noise. In this study, MSAC was used to delineate the specimen’s plane by specifying the maximum allowed distance and the maximum angular distance from the stationary point to the plane as well as setting a reference vector for that plane. For noise handling, the remaining noise from the previous step was removed by using the DBSCAN algorithm. The DBSCAN algorithm can remove uninterest regions with low point clouds density from the expected region of interest. Image binarization, also known as image thresholding, is a fundamental image processing technique used to convert a grayscale or color image into a binary image, where each pixel is assigned either a black or white value. The goal of image binarization is to separate the foreground objects (the objects of interest) from the background. The image binarization method was applied to the final extracted result, which included the background and specimen. Finally, the boundary of the specimen was generated by using a Sobel operator, which detected an edge on the binary images. Figure 12 shows the tracking points and the extracted boundary of the test specimen. Based on the extracted boundary of the test specimens, the vertical displacement of the beam–column joint was calculated as follows:

$$Y_{def} = (Y_{i+1} - Y_i) \times R_v \quad (1)$$

where Y_{def} is the deflection of the specimen (unit in mm); Y_{i+1} and Y_i are the tracking points at the Y axis of the i -th and $i + 1$ -th frames, respectively (unit in mm); and R_v is the vertical resolution (unit in mm).

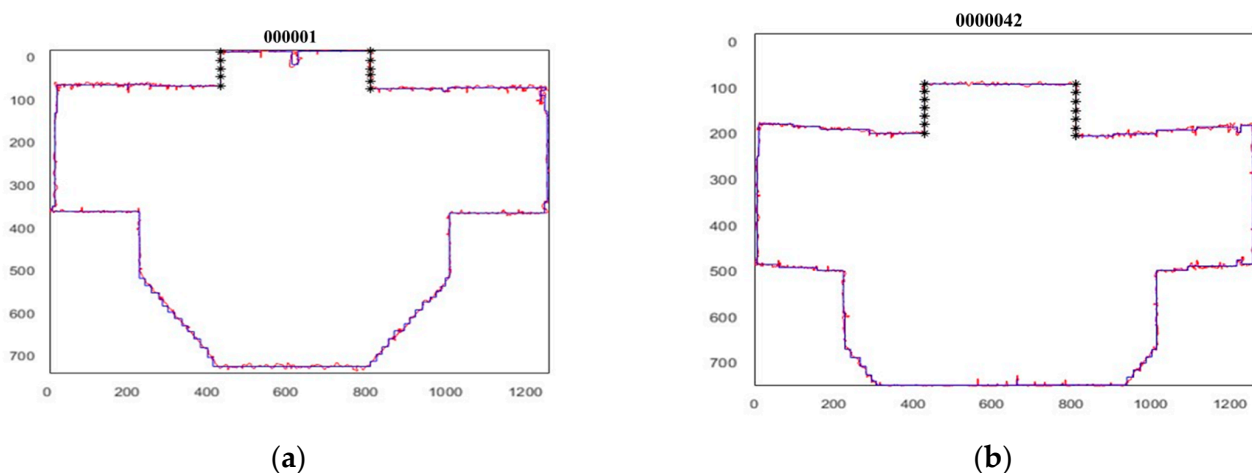


Figure 12. Tracking points for vertical displacement of the specimen: (a) PC-C; (b) PC-P.

Figure 13 directly compares the vertical displacement measured by the conventional LVDTs and the proposed LiDAR method. The vertical displacement measured by the LiDAR method is shown as a variation range, since it was calculated from all of the tracking points on the boundary of the specimen. Nevertheless, the tendency of vertical displacement was significantly similar regardless of the measurement method.

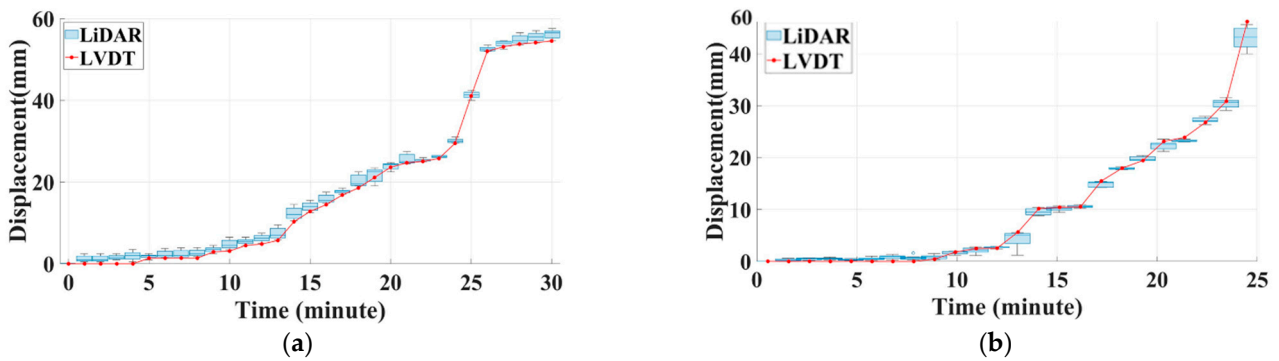


Figure 13. The displacement measurements during the experiments, showing the comparison between all point distributions by LiDAR (in boxes) and LVDTs: (a) PC-C; (b) PC-P.

4. Discussion

The correlation analysis between LVDT and LiDAR revealed that Wall A showed a high similarity of 99.73%, while Wall B had 98.86%, as shown in Figure 14. In both wall experiments, the displacement noise level of LiDAR was similar in size to the small displacement generated during the initial low lateral load application, resulting in an error with LVDT. However, for Wall B, the drift ratio between LiDAR and LVDT during the middle of the load application (110–160 min) showed an error of about 0.0028, as illustrated in Figure 14b. The LiDAR equipment scanned the left interface (reference to the rear of the wall) opposite the right wall equipped with LVDT #1. However, Wall B has an opening, which resulted in different behavior patterns on the left and right sides, leading to a low accuracy of 1%. When conducting a comparative experiment using an attached LVDT sensor through a LiDAR measuring instrument, which is a non-contact measurement method, excellent accuracy is expected.

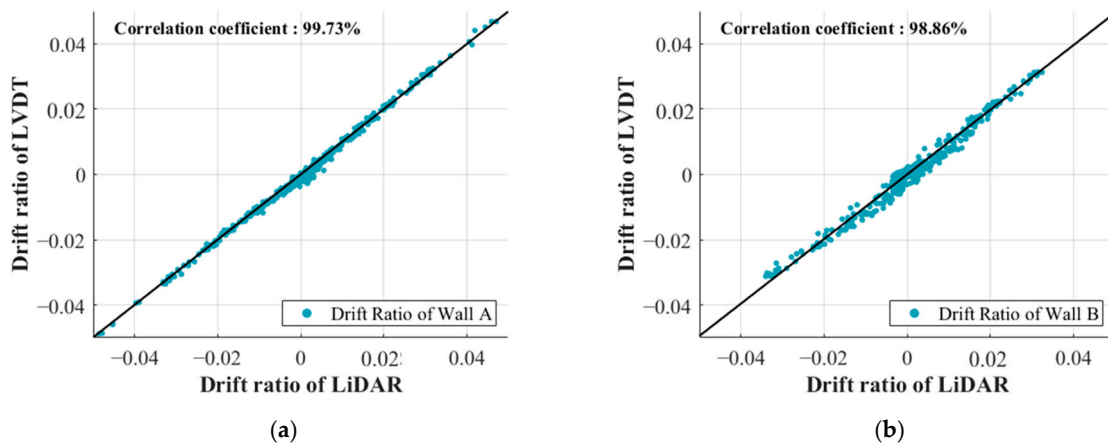


Figure 14. Drift ratio correlation between LVDT and extraction from LiDAR: (a) Wall A and (b) Wall B.

Figure 15 presents the correlation coefficient between the measurements obtained from LVDTs and LiDAR in vertical displacement. Notably, the correlation coefficient was calculated as 99.88% for the PC-C specimen and 99.94% for the PC-P specimen. The results indicated that the proposed method is totally reliable when comparing the measured LVDT data. This high correlation coefficient signifies a remarkably accurate relationship between the two measurement methods. In instances where the displacement values were relatively low, there was an observable increase in errors due to the presence of fine noise; this was particularly evident in situations involving low displacements. However, as the displacement values escalated, the accuracy of the measurements proportionally improved. This trend highlights the robustness of the LiDAR technique, particularly

for larger displacement values, while acknowledging its susceptibility to minor noise interference when measuring smaller displacements.

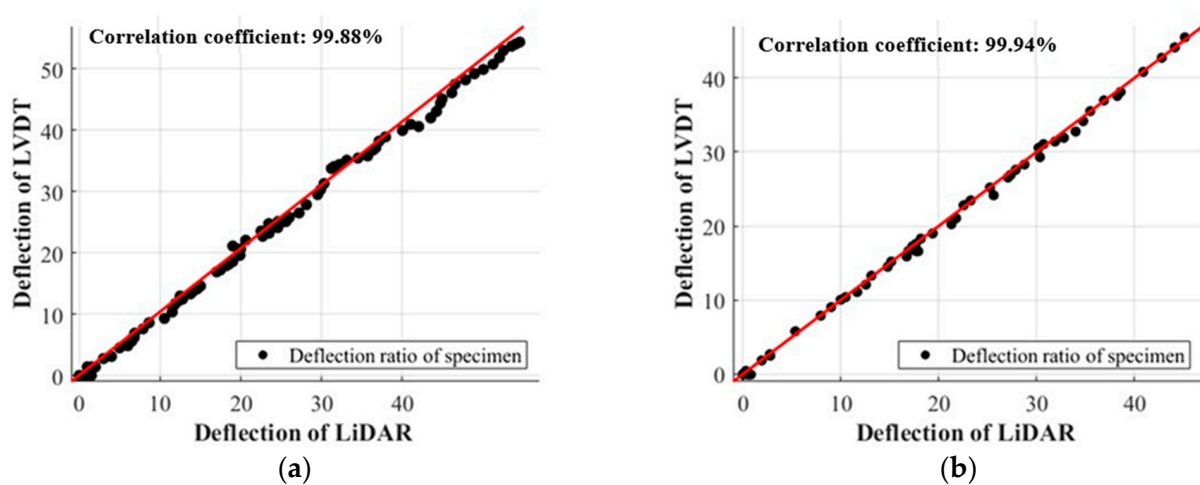


Figure 15. Displacement correlation between LVDT and extraction from LiDAR: (a) PC-C; (b) PC-P.

5. Conclusions

In this study, the displacement of concrete structures was measured through LiDAR, a non-contact sensor. An algorithm was developed to extract the lateral and vertical displacement of concrete structures from point clouds measured through LiDAR. The proposed method was compared with LVDT, the conventional contact-based sensor. The conclusions of this study are as follows:

- (1) With respect to the price, the LiDAR equipment applied in this study is affordable compared to contact-based measurement devices or cameras. Moreover, LiDAR has shown benefits compared to conventional devices such as saving time, being effective in structural failure conditions, and providing high-accuracy data with a resolution of approximately 1.0 mm.
- (2) The non-contact method was experimentally demonstrated in cases of the drift ratio of a concrete wall and the deflection of precast concrete, respectively. The results were compared with LVDT data. From the correlation analysis between LiDAR and LVDT, 99% similarity of the results was identified. This indicates that LiDAR data can be monitored to monitor specimens' deformation under loading in the same way as with the conventional method.
- (3) It is believed that a correlation error of 1–2% occurred in the point cloud extracted displacement value due to noise in the initial section. Further research needs to be conducted for plane fitting deformation through the advancement of the algorithm.

Author Contributions: Conceptualization, H.C. and U.W.; methodology, H.C.; software, D.K.; validation, T.T.P. and D.K.; investigation, T.T.P. and D.K.; resources, S.-G.J.; data curation, T.T.P. and D.K.; writing—original draft preparation, T.T.P. and D.K.; writing—review and editing, H.C.; visualization, U.W. and D.K.; supervision, H.C.; project administration, H.C.; funding acquisition, S.-G.J. All authors have read and agreed to the published version of the manuscript.

Funding: This research was funded by the Korea Agency for Infrastructure Technology Advancement (KAITA) grant funded by the Ministry of Land, Infrastructure and Transport (Grant RS-2022-00144050).

Institutional Review Board Statement: Not applicable.

Informed Consent Statement: Not applicable.

Data Availability Statement: The data presented and the MATLAB codes in this study are available upon request from the corresponding author.

Conflicts of Interest: The authors declare no conflict of interest.

References

1. Zuo, Z.; Huang, Y.; Pan, X.; Zhan, Y.; Zhang, L.; Li, X.; Zhu, M.; Zhang, L.; De Corte, W. Experimental research on remote real-time monitoring of concrete strength for highrise building machine during construction. *Measurement* **2021**, *13*, 109430. [[CrossRef](#)]
2. Farrar, C.R.; Allen, D.W.; Park, G.; Ball, S.; Masquelier, M.P. Coupling Sensing Hardware with Data Interrogation Software for Structural Health Monitoring. *Shock Vib.* **2006**, *13*, 519–530. [[CrossRef](#)]
3. Chang, F.; Markmiller, J.F.C.; Yang, J.; Kim, Y. Structural Health Monitoring. In *System Health Management*; Wiley: Hoboken, NJ, USA, 2011; pp. 419–428.
4. Farrar, C.R.; Worden, K. An Introduction to Structural Health Monitoring. *Philos. Trans. R. Soc. A Math. Phys. Eng. Sci.* **2007**, *365*, 303–315. [[CrossRef](#)] [[PubMed](#)]
5. Nazimko, V. Synchronization of the yield as a way to increase integrity and bearing capacity of the frame supports. *J. Struct. Integr. Maint.* **2022**, *7*, 1–14. [[CrossRef](#)]
6. Šedková, L.; Vlček, V.; Šedek, J. Delamination/disbond propagation analysis in adhesively bonded composite joints using guided waves. *J. Struct. Integr. Maint.* **2022**, *7*, 25–33.
7. Colombani, I.A.; Andrawes, B. A study of multi-target image-based displacement measurement approach for field testing of bridges. *J. Struct. Integr. Maint.* **2022**, *7*, 207–216. [[CrossRef](#)]
8. Sharma, S.; Dang, S.K.; Bairwa, S.K.; Sen, S. Comparative study on sensitivity of acceleration and strain responses for bridge health monitoring. *J. Struct. Integr. Maint.* **2022**, *7*, 238–251. [[CrossRef](#)]
9. Jo, H.C.; Kim, J.; Lee, K.; Sohn, H.-G.; Lim, Y.M. Non-Contact Strain Measurement for Laterally Loaded Steel Plate Using LiDAR Point Cloud Displacement Data. *Sens. Actuators A Phys.* **2018**, *283*, 362–374. [[CrossRef](#)]
10. Cabaleiro, M.; Riveiro, B.; Arias, P.; Caamaño, J.C. Algorithm for Beam Deformation Modeling from LiDAR Data. *Measurement* **2015**, *76*, 20–31. [[CrossRef](#)]
11. Sun, L.; Abolhasannejad, V.; Gao, L.; Li, Y. Non-Contact Optical Sensing of Asphalt Mixture Deformation Using 3D Stereo Vision. *Measurement* **2016**, *85*, 100–117. [[CrossRef](#)]
12. Maru, M.B.; Lee, D.; Cha, G.; Park, S. Beam Deflection Monitoring Based on a Genetic Algorithm Using Lidar Data. *Sensors* **2020**, *20*, 2144. [[CrossRef](#)] [[PubMed](#)]
13. Kang, X.; Li, J.; Fan, X.; Wan, W. Real-time rgb-d simultaneous localization and mapping guided by terrestrial lidar point cloud for indoor 3-d reconstruction and camera pose estimation. *Appl. Sci.* **2019**, *9*, 3264. [[CrossRef](#)]
14. Kim, J.S.; Lee, G.Y.; Kim, Y.S. 2D-LiDAR-Sensor-Based Retaining Wall Displacement Measurement System. *Appl. Sci.* **2022**, *12*, 11335. [[CrossRef](#)]
15. Lee, J.; Jo, H.; Oh, J. Application of Drone LiDAR Survey for Evaluation of a Long-Term Consolidation Settlement of Large Land Reclamation. *Appl. Sci.* **2023**, *13*, 8277. [[CrossRef](#)]
16. Tang, P.; Akinci, B.; Huber, D. Quantification of edge loss of laser scanned data at spatial discontinuities. *Autom. Constr.* **2009**, *18*, 1070–1083. [[CrossRef](#)]
17. Tang, P.; Huber, D.; Akinci, B. A comparative analysis of depth-discontinuity and mixed-pixel detection algorithms. In Proceedings of the Sixth International Conference on 3-D Digital Imaging and Modeling (3DIM 2007), Montreal, QC, Canada, 21–23 August; IEEE: Piscataway, NY, USA, 2007; pp. 29–38.
18. Liu, X. Airborne LiDAR for DEM Generation: Some Critical Issues. *Prog. Phys. Geogr. Earth Environ.* **2008**, *32*, 31–49. [[CrossRef](#)]
19. Kukko, A.; Hyyppä, J. Small-Footprint Laser Scanning Simulator for System Validation, Error Assessment, and Algorithm Development. *Photogramm. Eng. Remote Sens.* **2009**, *75*, 1177–1189. [[CrossRef](#)]
20. Zhang, H.; Duan, Z.; Zheng, N.; Li, Y.; Zeng, Y.; Shi, W. An Efficient Class-Constrained DBSCAN Approach for Large-Scale Point Cloud Clustering. *IEEE J. Sel. Top. Appl. Earth Obs. Remote Sens.* **2022**, *15*, 7323–7332. [[CrossRef](#)]
21. Chen, H.; Liang, M.; Liu, W.; Wang, W.; Liu, P.X. An approach to boundary detection for 3D point clouds based on DBSCAN clustering. *Pattern Recognit.* **2022**, *124*, 108431. [[CrossRef](#)]
22. Montgomery, D.C.; Peck, E.A.; Vining, G.G. *Introduction to Linear Regression Analysis*; John Wiley & Sons: Hoboken, NJ, USA, 2021.
23. Kim, S.-H.; Kim, H.-D.; Kang, S.-M.; Hwang, H.-J.; Choi, H. Effect of Joint Details on Progressive Collapse Resistance of Precast Concrete Structures. *J. Build. Eng.* **2023**, *69*, 106217. [[CrossRef](#)]

Disclaimer/Publisher’s Note: The statements, opinions and data contained in all publications are solely those of the individual author(s) and contributor(s) and not of MDPI and/or the editor(s). MDPI and/or the editor(s) disclaim responsibility for any injury to people or property resulting from any ideas, methods, instructions or products referred to in the content.